

**Aerosol extinction to
backscatter ratio
from passive satellite
measurements**

F.-M. Bréon

Aerosol extinction to backscatter ratio derived from passive satellite measurements

F.-M. Bréon

Laboratoire des Sciences du Climat et de l'Environnement, CEA/DSM/LSCE, UMR8212,
CEA-CNRS-UVSQ, 91191 Gif sur Yvette, France

Received: 19 December 2012 – Accepted: 8 January 2013 – Published: 22 January 2013

Correspondence to: F.-M. Bréon (fmbreon@cea.fr)

Published by Copernicus Publications on behalf of the European Geosciences Union.

[Title Page](#)[Abstract](#)[Introduction](#)[Conclusions](#)[References](#)[Tables](#)[Figures](#)[⏪](#)[⏩](#)[◀](#)[▶](#)[Back](#)[Close](#)[Full Screen / Esc](#)[Printer-friendly Version](#)[Interactive Discussion](#)

Abstract

Spaceborne reflectance measurements from the POLDER instrument are used to study the specific directional signature close to the backscatter direction. The data analysis makes it possible to derive the extinction to backscatter ratio (EBR) which is the invert of the scattering phase function for an angle of 180° and is needed for a quantitative interpretation of lidar observations (active measurements). In addition, the multi-directional measurements are used to quantify the scattering phase function variations close to backscatter, which also provide some indication of the aerosol particle size and shape. The spatial distributions of both parameters show consistent patterns that are consistent with the aerosol type distributions. Pollution aerosols have an EBR close to 70, desert dust values are on the order of 50, while marine aerosol's is close to 25. The scattering phase function shows an increase with the scattering angle close to backscatter. The relative increase $\partial \ln P / \partial \gamma$ is close to 0.01 for dust and pollution type aerosols and 0.06 for marine type aerosols. These values are consistent with those retrieved from Mie simulations.

1 Introduction

Atmospheric scattering contributes to the Top Of the Atmosphere (TOA) reflectance. The directional signature, i.e. how the reflectance varies with the viewing geometry, depends on the scattering phase function of atmospheric particles: molecules, aerosols and cloud droplets. This signature can be used for an estimate of the scatterer size distribution (Deuzé et al., 2000; Bréon and Doutriaux, 2005; Mayer et al., 2004) and shape (Herman et al., 2005). Of particular interest is the backscattering direction that shows some specific signatures, in particular the well-known glory (Spinhirne and Nakajima, 1994) or the antisolar maximum (Sherwood et al., 2005).

Accurate scattering phase functions are needed to relate the measured atmosphere reflectance to the atmospheric load in aerosol and clouds (i.e. their optical thickness).

ACPD

13, 2351–2370, 2013

Aerosol extinction to backscatter ratio from passive satellite measurements

F.-M. Bréon

Title Page

Abstract

Introduction

Conclusions

References

Tables

Figures

⏪

⏩

◀

▶

Back

Close

Full Screen / Esc

Printer-friendly Version

Interactive Discussion



**Aerosol extinction to
backscatter ratio
from passive satellite
measurements**

F.-M. Bréon

Title Page

Abstract

Introduction

Conclusions

References

Tables

Figures

⏪

⏩

◀

▶

Back

Close

Full Screen / Esc

Printer-friendly Version

Interactive Discussion

For the interpretation of lidar returns in terms of extinction, it is necessary to know the extinction to backscatter ratio (EBR), also referred to as the Lidar Ratio, i.e. the phase function for the 180° scattering angle. For spherical particles such as water droplets, or aerosols that are small with respect to wavelength, the Mie theory enables to calculate accurate scattering phase functions. On the other hand, no such accurate and efficient method exists for non-spherical particles, in particular because their real shape is not properly known. There have been attempts to approximate the shape of non-spherical particles as spheroids (Mishchenko et al., 1997), hexagonal crystals (C.-Labonnote et al., 2001) or more complex shapes (Macke et al., 1996). Such simulations show that the EBR for non-spherical dust particles is significantly larger than that of spherical particles with the same size distribution (e.g. Dubovik et al., 2006; Veselovskii et al., 2010).

Empirical phase functions for non-spherical particles are also available derived from laboratory measurements (Volten et al., 2004). These scattering matrices are given as a function of angle in the range $5\text{--}173^\circ$, at the wavelengths of 441.6 nm and 632.8 nm and for several irregularly shaped mineral aerosol particles such as Sahara sand. Unfortunately, there is no information for the largest scattering angles due to the difficulty of having the light source and the detector in the same direction. One objective of the present paper is to fill this gap: based on satellite measurements of the atmosphere reflectance, we analyze the phase function variations in the range $170\text{--}180^\circ$.

The PARASOL satellite was launched in December 2004 to be part of the so-called A-Train (Tanré et al., 2011; Anderson et al., 2005). The platform carries the POLDER radiometer (Deschamps et al., 1994), which was flown earlier onboard the ADEOS-I and II satellites. It provides global systematic measurements of the spectral, directional, and polarization characteristics of the solar radiation reflected by the Earth/atmosphere system. The wide bi-dimensional field of view permits the observation of the backscatter direction continuously over the tropics and mid-latitude regions. It is therefore well-suited to study the reflectance backscatter signature as was shown for land surface targets in Bréon et al. (2002). In this paper, we focus on the signatures generated by

aerosol scattering. We have processed four years of PARASOL observations acquired in the backscatter direction (several thousands cases), which provides a large statistics of directional signatures.

Section 2 describes the data analysis method. Section 3 shows the results and provides some interpretation. Section 4 discusses the results and concludes.

2 Data and method

The POLDER instrument is composed of a wide field-of-view lens, a filter wheel and a detector. The filter wheel permits radiance measurements in eight spectral bands from 440 nm (blue) to 1020 nm (near IR). The detector is a bi-dimensional CCD array with 242×274 independent sensitive areas. One snapshot provides an image of a portion of the Earth of size roughly $1900 \times 1400 \text{ km}^2$, similar to what a camera with a wide field-of-view lens would provide, with a spatial resolution on the order of 6 km. The pixels in the image are viewed with various zenith angles and azimuths. The zenith angle at the surface varies between 0° at the image center, to 50° crosstrack and 60° forward and aft.

One snapshot is acquired, for each spectral band, every 20 s. There is a large overlap of the areas observed by successive snapshots. Thus a given target is observed from varying directions as the satellite goes along its orbit. The reflectance of a target in the instrument swath is acquired between 12 and 16 times depending on its position with respect to the satellite subtrack. In most cases, depending on the solar position with respect to the satellite, there is one pixel that is observed exactly (at the POLDER pixel angular resolution) in the backscatter geometry. This pixel is where the shadow of the satellite would be seen if it were much larger. The viewing geometry corresponds to a scattering angle of 180° , which is the same as for a lidar observation. The view zenith angle (VZA) is different however; it is generally close to zero for a lidar (the current CALIPSO observations have a VZA of 3°) while POLDER VZA for backscatter pixels is equal to the sun zenith angle.

Aerosol extinction to backscatter ratio from passive satellite measurements

F.-M. Bréon

Title Page

Abstract

Introduction

Conclusions

References

Tables

Figures



Back

Close

Full Screen / Esc

Printer-friendly Version

Interactive Discussion



Aerosol extinction to backscatter ratio from passive satellite measurements

F.-M. Bréon

Title Page

Abstract

Introduction

Conclusions

References

Tables

Figures

⏪

⏩

◀

▶

Back

Close

Full Screen / Esc

Printer-friendly Version

Interactive Discussion



We have processed the full set of spaceborne POLDER/PARASOL measurements available at the time of this study. For each sequence of acquisition (one sequence every 20 s), we identified the surface pixel that is observed in the backscattering direction. This pixel is also observed from a number of other sequences/directions that are used to measure the directional signature for a wide range of scattering angles (see Fig. 1). These directions can be used for an estimate of the aerosol scattering phase function over this range. The spectral and directional signatures of the reflectance provide the necessary information to constrain both the aerosol optical thickness and the aerosol model in an inversion procedure (Deuzé et al., 2000).

In practice, the aerosol inversion procedure uses a set of bimodal aerosol models. The optical depth and the radii of the fine and coarse modes are inverted based on a best fit between the measurements and the radiative transfer simulations. A non-sphericity index is also adjusted for the coarse mode. The output of this operational inversion is an aerosol model and a spectral optical depth. The quality of the fit between the measurements and the modeling is quantified in a quality index. The optical depth retrievals have been validated against sunphotometer measurements (e.g. Bréon et al., 2011).

The set of aerosol models used for the inversion is wide but limited. It is based on log-normal number distributions with a unique refractive index and there is a single empirical model for non-spherical particles. As a consequence, the inverted model and its scattering phase functions are only an approximation of the reality. The residual between the measurements and the modeling can be used to correct the scattering phase function:

The single scattering contribution to the reflectance can be modeled analytically

$$R_{ss}(\mu_s, \mu_v, \phi) = \frac{1 - \exp\left[-\tau\left(\frac{1}{\mu_s} + \frac{1}{\mu_v}\right)\right]}{4(\mu_s + \mu_v)} \omega P(\gamma) \quad (1)$$

$$\approx \frac{\omega \tau P(\gamma)}{4\mu_s \mu_v}$$

where τ is the aerosol optical depth, ω is the single scattering albedo, μ_s and μ_v are the cosine of the solar and view zenith angles respectively, and γ is the scattering angle which can be computed from the zenith angles and the relative azimuth:

$$-\cos(\gamma) = \mu_s \mu_v + \sqrt{(1 - \mu_s^2)(1 - \mu_v^2)} \cos \phi \quad (2)$$

5 The main assumption is that the modelling provides a good approximation of the reality. It can therefore be used to estimate second order terms, including scattering by atmospheric molecules, surface contribution and multiple scattering. The measurement-model misfit is affected to the single scattering contribution only. One can then make a corrected estimate of the scattering phase function

$$10 P_{\text{aer}}(\gamma) = P_{\text{mod}}(\gamma) + \frac{4\mu_s\mu_v}{\omega\tau} [R_{\text{mes}}(\mu_s, \mu_v, \phi) - R_{\text{mod}}(\mu_s, \mu_v, \phi)] \quad (3)$$

where P_{mod} is the scattering phase function of the retrieved aerosol model, R_{mod} is the TOA reflectance computed for the retrieved aerosol model and optical depth and R_{mes} are the measurements. Note that R_{mes} is acquired in an atmospheric window, relatively free of atmospheric absorption, and that the small absorption has been corrected as described in Deuzé et al. (2000).

15 The operational processing of POLDER data includes the derivation of P_{aer} as described above. This is done for all pixels for which there is a successful aerosol retrieval, although this parameter is not included in the operational product that is widely distributed. We have had access to the restricted product and have extracted all pixels that include one observation in the backscatter direction.

20 In the following, we analyze the values of $P_{\text{aer}}(\gamma)$ close to backscattering ($\gamma \approx 180^\circ$). One parameter of interest is the value of the phase function for $\gamma = 180^\circ$. This value is of particular interest to relate to lidar observations. Rather than the phase function itself, the lidar community uses the so-called Lidar Ratio, which is the extinction to backscatter ratio $4\pi/(\omega P(180))$. We therefore show our results expressed as the EBR.

Aerosol extinction to backscatter ratio from passive satellite measurements

F.-M. Bréon

Title Page

Abstract

Introduction

Conclusions

References

Tables

Figures

⏪

⏩

◀

▶

Back

Close

Full Screen / Esc

Printer-friendly Version

Interactive Discussion



In addition, we analyze how the phase function varies close to backscattering. Mie simulations indicate that the scattering phase functions increases sharply as the angle increases towards 180° (see examples in Fig. 3). POLDER multidirectional measurements can be used to confirm this observation. We make use of the measurement sequences preceding and following that acquired in the backscatter geometry (difference in time of ≈ 20 s). We want to quantify the relative variation of the phase function per degree. The derivative of the phase function is approximated from two succeeding measurements using that observed at backscatter and either the preceding or the following ones:

$$\begin{aligned}
 V &= \frac{1}{P_{\text{aer}}} \left. \frac{\partial P_{\text{aer}}}{\partial \gamma} \right|_{\gamma=180^\circ} \\
 &= \left. \frac{\partial \ln(P_{\text{aer}})}{\partial \gamma} \right|_{\gamma=180^\circ} \\
 &\approx \frac{\ln P_{\text{aer}}(180) - \ln P_{\text{aer}}(\gamma)}{180 - \gamma}
 \end{aligned} \tag{4}$$

3 Results

Figure 3 shows the results of simple Mie simulations. The scattering phase function is shown for 5 log-normal size distribution with a fixed width and a range of modal radius. For the smallest aerosol, the phase function is almost flat (black line) and its value at backscatter is ≈ 0.66 . For intermediate aerosol sizes (modal radii of $0.1\text{--}0.3\ \mu\text{m}$) the phase function at backscatter is fairly flat and the backscatter value is close to 0.2. For larger aerosol (modal radius of $1\ \mu\text{m}$ and larger) the phase function shows large increases towards backscatter and reaches a value larger than 0.7. These backscatter values corresponds to BER between 19 and 63 which are in the typical range of reported values (e.g. Doherty et al., 1999; Burton et al., 2012). As for the slope at backscatter, Fig. 3 shows that scattering phase functions show irregular variations. As

Aerosol extinction to backscatter ratio from passive satellite measurements

F.-M. Bréon

Title Page

Abstract

Introduction

Conclusions

References

Tables

Figures



Back

Close

Full Screen / Esc

Printer-friendly Version

Interactive Discussion



a consequence, the slope computed from two directional samples, one at 180° and the other at another angle between 170 and 175° , will depend on the latter. There is nevertheless a clear tendency for an increase of V from the fine mode aerosols to the largest particles. Typical values vary between 0 and 0.1.

In a recent paper, Burton et al. (2012), hereafter referred to as BU12, report on Raman lidar measurements acquired in a wide range of conditions. They show typical values of the lidar ratio and other aerosol optical parameters as a function of the aerosol type. Maritime aerosol have lidar ratio of 20 ± 10 , dust is 45 ± 15 , while smoke and urban are 70 ± 15 . For the processing of the spaceborne CALIPSO observations, six aerosol types have been defined and a priori values of the lidar ratio are used for each of them (Omar et al., 2009). These are clean continental, clean marine, dust, polluted continental, polluted dust, and smoke, with 532 nm (1064 nm) EBR of 35 (30), 20 (45), 40 (55), 70 (30), 65 (30), and 70 (40), respectively.

Figure 4 shows seasonal maps of the lidar ratio derived from POLDER measurements at 670 nm. We only show cases when the retrieved optical depth is larger than 0.1 and smaller than 0.4. The smaller optical depth values are excluded because one needs some aerosol signal. The largest values are excluded as the multiple scattering becomes dominant and may prevent an accurate determination of the single scattering contribution. Because of these restrictions, there are some white areas in the global maps with no valid retrievals. On the other hand, there are also some very clear spatial and temporal features, which indicates that there is some information in the measurements. The smallest lidar ratios are found over the open oceans with typical values around 25. These are clearly consistent with the values reported by BU12 for Maritime aerosols as well as the value of 20 used by the CALIPSO operational processing for clean marine aerosols. At the other extreme, the largest values are on the order of 75 and found around the coast of India during the Dec-Feb season. This area is known to be loaded with pollution aerosols from the India subcontinent. Again, these large values are consistent with those reported in BU12 for the urban aerosol and those selected for CALIPSO for the “polluted continental case”. EBR on the order of 60 are observed

Aerosol extinction to backscatter ratio from passive satellite measurements

F.-M. Bréon

[Title Page](#)[Abstract](#)[Introduction](#)[Conclusions](#)[References](#)[Tables](#)[Figures](#)[⏪](#)[⏩](#)[◀](#)[▶](#)[Back](#)[Close](#)[Full Screen / Esc](#)[Printer-friendly Version](#)[Interactive Discussion](#)

**Aerosol extinction to
backscatter ratio
from passive satellite
measurements**

F.-M. Bréon

Title Page

Abstract

Introduction

Conclusions

References

Tables

Figures

⏪

⏩

◀

▶

Back

Close

Full Screen / Esc

Printer-friendly Version

Interactive Discussion

over areas where biomass burning aerosols are expected, such as the gulf of Guinea during December–February, and further south during June–August. As for dust, this aerosol type is prevalent around the Saharan desert, including the Mediterranean, during the summer season. For this area, our result indicates lidar ratio close to 50, again very consistent with the BU12 values but significantly larger than those used for the CALIPSO processing (40). However, recent work (e.g. Schuster, 2012) indicates that the selected value is too low and that higher values should be used although regional variations are observed. The uncertainty on the dust BER results from the refractive index variability (Schuster et al., 2012) and the non-spherical nature of the particles (Veselovskii et al., 2012).

Therefore, over areas with well-defined aerosol types, the POLDER retrievals of the lidar ratio are similar to the expected values, which generates some confidence in the results.

Figure 5 shows the derivative of the phase function V (see Eq. 4) for the same data points as in Fig. 4. This figure shows very clear spatial and temporal patterns, some of which are not apparent on the EBR retrievals. This observation clearly indicates that there is some information on the prevalent aerosol type that is not in the backscatter values. The derivative varies between 0.01 and 0.07 deg^{-1} which is similar to the values from the Mie simulations shown in Fig. 3. The smallest values are found in coastal areas in regions that are affected by urban, biomass burning or dust type aerosols. Such low values of the derivative V are consistent with the Mie simulation results for small particles (Fig. 3). Conversely, the largest values are found over the open oceans. However, there is a clear zonal and seasonal gradient and the large values of V are not observed over the tropics but only at mid and high latitudes. Regions affected by dust shows unexpected values. As rather coarse particles, one would expect slopes in the high range based on Mie simulations. Values retrieved downwind of the Sahara are smaller than 0.03 which is not consistent with the results of Mie simulations such as those of Fig. 3. We hypothesize that this inconsistency results from the non-spherical

nature of the dust particles. Our measurement of the slope V could be used to constrain the aerosol microphysics and in particular the non-spherical nature of the particles.

In general, there is an inverse relationship between V and the EBR (Fig. 6). Regions with the largest EBR (> 50) show V on the order of 0.02. For the smaller EBR (< 50) which are mostly observed over the remote oceans, V is generally greater than 0.04, with a significant range up to about 0.07. The range seems to have a zonal and temporal dependency, as illustrated in Fig. 5.

4 Discussion and conclusions

The POLDER instrument onboard the PARASOL satellite is the only spaceborne instrument that provides measurements of the phase function variation at and close to backscatter. Although the MISR instrument (Diner et al., 1999) onboard the Terra satellite does provide multidirectional observations, its viewing geometry does not sample the backscatter direction. The measurements shown in this short paper are therefore unique and it is the first time, to our knowledge, that the POLDER measurements have been processed to analyze the BER and the directional signature of the measurements close to backscatter.

Although the POLDER instrument does provide measurements in the anti-solar (backscatter) direction, these observations are relatively rare. Let us recall that the POLDER measurement principle is that of a very wide field of view that acquires one shot for each spectral band every ≈ 20 s. For each such acquisition, there is one point on Earth that is observed in the backscatter direction. As a consequence, the backscatter sampling per day is 14.5 (the number of orbits) roughly north-south sets of observations, distant by 25° of longitude, each set providing observations distant by ≈ 140 km (the distance travelled by the satellite during the 20 s). A large fraction of these measurements are not suitable for the analysis developed in this paper either because of cloud contamination or an insufficient aerosol load. As a consequence, the number of valid observation is relatively small compared to what is typically achieved through

Aerosol extinction to backscatter ratio from passive satellite measurements

F.-M. Bréon

Title Page

Abstract

Introduction

Conclusions

References

Tables

Figures

⏪

⏩

◀

▶

Back

Close

Full Screen / Esc

Printer-friendly Version

Interactive Discussion



spaceborne remote sensing. We have therefore limited the analysis to climatological distribution and made no attempt to relate the retrieved values to other concomitant measurements.

Nevertheless, the spatial and temporal structures of both the EBR and phase function slope (V) show clear patterns that can be related to the known distribution of aerosol types in the atmosphere. In addition, the retrieved EBR are very consistent with the typical values measured with a Raman lidar in various environments and the generally accepted values for various aerosol types (Doherty et al., 1999; Omar et al., 2009; Burton et al., 2012). Therefore, although we could not offer a quantitative validation of our estimates, they clearly contain some information about the aerosol. These data can be used to generate a climatology of aerosol EBR, which is necessary to process the measurements of backscatter lidar such as CALIPSO. Our observations generally confirm recent results that the EBR used for dust is too low (Schuster et al., 2012). As for V , results of Mie simulations of the phase function close to backscatter show a high sensitivity to the aerosol size distribution. The general shape of the scattering phase function is also very sensitive to the non-spherical natures of the particles such as dust. The retrieved V values could therefore be used as a further constraint to characterize the microphysical properties of the aerosols. However, because of the scarcity of proper backscatter observations, this can be done only in a climatological way.

Acknowledgements. The data used in this paper were derived from the measurements of the CNES POLDER instrument onboard the PARASOL micro-satellite. The data processing was made easy thanks to the facilities provided by the ICARE thematic center www.icare.univ-lille1.fr.

Aerosol extinction to backscatter ratio from passive satellite measurements

F.-M. Bréon

Title Page

Abstract

Introduction

Conclusions

References

Tables

Figures



Back

Close

Full Screen / Esc

Printer-friendly Version

Interactive Discussion



The publication of this article is financed by CNRS-INSU.

References

- Anderson, T. L., Charlson, R. J., Bellouin, N., Boucher, O., Chin, M., Christopher, S. A., Haywood, J., Kaufman, Y. J., Kinne, S., Ogren, J. A., Remer, L. A., Takemura, T., Tanré, D., Torres, O., Trepte, C. R., Wielicki, B. A., Winker, D. M., and Yu, H.: An “A-Train” strategy for quantifying direct climate forcing by anthropogenic aerosols, *B. Am. Meteorol. Soc.*, 86, 1795–1809, 2005.
- Bréon, F.-M, and Doutriaux-Boucher, M.: A comparison of cloud droplet radii measured from space, *IEEE T. Geosci. Remote*, 43, 1796–1805, 2005.
- Bréon, F.-M, Vermeulen, A., and Descloitres, J.: An evaluation of satellite aerosol products against sunphotometer measurements, *Remote Sens. Environ.*, 115, 3102–3111, 2011.
- Burton, S. P., Ferrare, R. A., Hostetler, C. A., Hair, J. W., Rogers, R. R., Obland, M. D., Butler, C. F., Cook, A. L., Harper, D. B., and Froyd, K. D.: Aerosol classification using airborne High Spectral Resolution Lidar measurements – methodology and examples, *Atmos. Meas. Tech.*, 5, 73–98, doi:10.5194/amt-5-73-2012, 2012.
- C.-Labonnote, L., Brogniez, G., Buriez, J.-C., Doutriaux-Boucher, M., Gayet, J.-F., and Macke, A.: Polarized light scattering by inhomogeneous hexagonal monocrystals. Validation with ADEOS-POLDER measurements, *J. Geophys. Res.*, 106, 12139–12153, 2001.
- Deschamps, P.-Y., Buriez, J.-C., Bréon, F.-M., Leroy, M., Podaire, A., Bricaud, A., and Seze, G.: The POLDER Mission – instrument characteristics and scientific objectives (polarization and directionality of Earth’s reflectances), *IEEE T. Geosci. Remote*, 32, 598–615, 1994.
- Deuzé, J. L., Goloub, P., Herman, M., Marchand, A., Perry, G., Susana, S., and Tanré, D.: Estimate of the aerosol properties over the ocean with POLDER on ADEOS-1, *J. Geophys. Res.*, 105, 15329–15346, 2000.

Aerosol extinction to backscatter ratio from passive satellite measurements

F.-M. Bréon

Title Page

Abstract

Introduction

Conclusions

References

Tables

Figures



Back

Close

Full Screen / Esc

Printer-friendly Version

Interactive Discussion



Aerosol extinction to backscatter ratio from passive satellite measurements

F.-M. Bréon

Title Page

Abstract

Introduction

Conclusions

References

Tables

Figures

⏪

⏩

◀

▶

Back

Close

Full Screen / Esc

Printer-friendly Version

Interactive Discussion



Diner, D. J., Asner, G. P., Davies, R., Knyazikhin, Y., Muller, J.-P., Nolin, A. W., Pinty, B., Schaaf, C. B., and Stroeve, J.: New directions in earth observing: scientific applications of multiangle remote sensing, *B. Am. Meteorol. Soc.*, 80, 2209–2228, 1999.

Doherty, S., Anderson, T. L., and Charlson, R. J.: Measurement of the lidar ratio for atmospheric aerosols with a 180° backscatter nephelometer, *Appl. Optics*, 38, 1823–1832, 1999.

Dubovik, O., Sinyuk, A., Lapyonok, T., Holben, B. N., Mishchenko, M., Yang, P., Eck, T. F., Volten, H., Muñoz, O., Veihelmann, B., van der Zande, J., Leon, J.-F., Sorokin, M., and Slutsker, I.: Application of spheroid models to account for aerosol particle nonsphericity in remote sensing of desert dust, *J. Geophys. Res.*, 111, D11208, doi:10.1029/2005JD006619, 2006.

Herman, M., Deuzé, J.-L., Marchand, A., Roger, B., and Lallart, P.: Aerosol remote sensing from POLDER/ADEOS over the ocean: improved retrieval using a nonspherical particle model, *J. Geophys. Res.*, 110, D10S02, doi:10.1029/2004JD004798, 2005.

Josset, D., Rogers, R., Pelon, J., Hu, Y., Liu, Z., Omar, A., and Zhai, P.-W.: CALIPSO lidar ratio retrieval over the ocean, *Opt. Express*, 19, 18696–18706, 2011.

Macke, A., Mueller, J., and Raschke, E.: Single scattering properties of atmospheric ice crystals, *J. Atmos. Sci.*, 53, 2813–2825, 1996.

Mayer, B., Schröder, M., Preusker, R., and Schüller, L.: Remote sensing of water cloud droplet size distributions using the backscatter glory: a case study, *Atmos. Chem. Phys.*, 4, 1255–1263, doi:10.5194/acp-4-1255-2004, 2004.

Mishchenko, M. I., Travis, L. D., Kahn, R. A., and West, R. A.: Modeling phase functions for dustlike tropospheric aerosols using a shape mixture of randomly oriented polydisperse spheroids, *J. Geophys. Res.*, 102, 16831–16847, 1997.

Omar, A. H., Winker, D. M., Vaughan, M. A., Hu, Y., Trepte, C. R., Ferrare, R. A., Lee, K.-P., Hostetler, C. A., Kittaka, C., Rogers, R. R., Kuehn, R. E., and Liu, Z.: The CALIPSO automated aerosol classification and lidar ratio selection algorithm, *J. Atmos. Ocean. Techn.*, 26, 1994–2014, doi:10.1175/2009JTECHA1231.1, 2009.

Schuster, G. L., Vaughan, M., MacDonnell, D., Su, W., Winker, D., Dubovik, O., Lapyonok, T., and Trepte, C.: Comparison of CALIPSO aerosol optical depth retrievals to AERONET measurements, and a climatology for the lidar ratio of dust, *Atmos. Chem. Phys.*, 12, 7431–7452, doi:10.5194/acp-12-7431-2012, 2012.

Sherwood, S. C.: Detection of faceted crystals in deep convective clouds via the antisolar peak, *J. Geophys. Res.*, 110, D14205, doi:10.1029/2004JD005549, 2005.

- Spinhirne, J. D. and Nakajima, T.: Glory of clouds in the near infrared, *Appl. Optics*, 33, 4652–4662, 1994.
- Tanré, D., Bréon, F. M., Deuzé, J. L., Dubovik, O., Ducos, F., François, P., Goloub, P., Herman, M., Lifermann, A., and Waquet, F.: Remote sensing of aerosols by using polarized, directional and spectral measurements within the A-Train: the PARASOL mission, *Atmos. Meas. Tech.*, 4, 1383–1395, doi:10.5194/amt-4-1383-2011, 2011.
- Volten, H., Munoz, O., Rol, E., de Haan, J. F., Vassen, W., Hovenier, J. W., Muinonen, K., and Nousiainen T.: Scattering matrices of mineral aerosol particles at 441.6 nm and 632.8 nm, *J. Geophys. Res.*, 106, 375–401, 2001.
- Veselovskii, I., Dubovik, O., Kolgotin, A., Lapyonok, T., Di Girolamo, P., Summa, D., Whiteman, D. N., Mishchenko, M., and Tanré, D.: Application of randomly oriented spheroids for retrieval of dust particle parameters from multiwavelength lidar measurements, *J. Geophys. Res.*, 115, D21203, doi:10.1029/2010JD014139, 2010.
- Young, S. and Vaughan, M.: The retrieval of profiles of particulate extinction from cloud-aerosol lidar infrared pathfinder satellite observations (CALIPSO) data: algorithm description, *J. Atmos. Tech.*, 26, 1105–1119, 2009.

Aerosol extinction to backscatter ratio from passive satellite measurements

F.-M. Bréon

[Title Page](#)[Abstract](#)[Introduction](#)[Conclusions](#)[References](#)[Tables](#)[Figures](#)[⏪](#)[⏩](#)[◀](#)[▶](#)[Back](#)[Close](#)[Full Screen / Esc](#)[Printer-friendly Version](#)[Interactive Discussion](#)

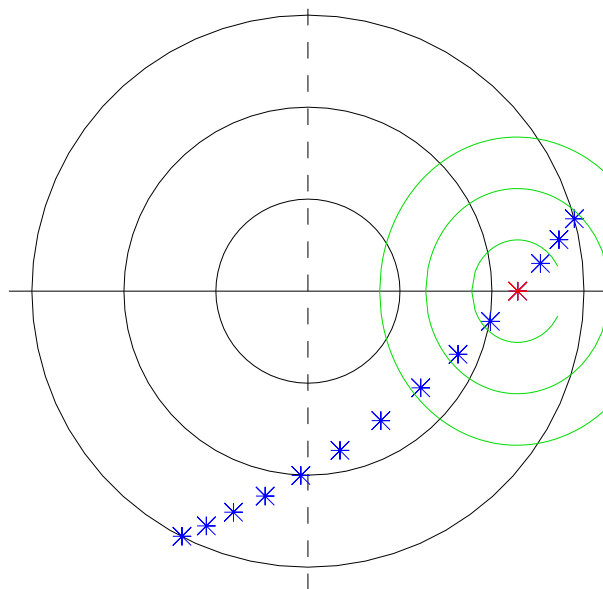


Fig. 1. Typical geometry by PARASOL multi-directional observations for a pixel that is observed in the backscatter direction. The black circles show the view angle by step of 20° , the straight plain line shows the principal plane while the dashed line shows the perpendicular plane. The green ellipses show the scattering angles by step of 10° . Each symbols indicates the viewing geometry of one of the 14 successive observations. The red symbol shows the observation acquired in the near backscatter direction.

Aerosol extinction to backscatter ratio from passive satellite measurements

F.-M. Bréon

Title Page	
Abstract	Introduction
Conclusions	References
Tables	Figures
◀	▶
◀	▶
Back	Close
Full Screen / Esc	
Printer-friendly Version	
Interactive Discussion	



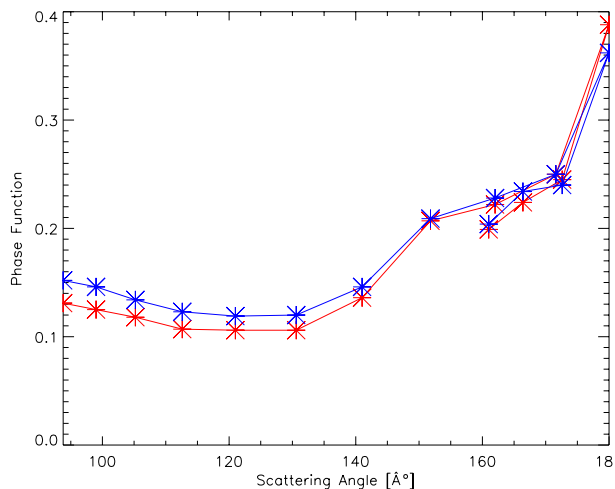


Fig. 2. Phase function retrieved from PARASOL measurements for the same pixel as in Fig. 1. Red (blue) is for the 670 nm (865 nm) band. Note that, for the largest scattering angles, there are two measurements for similar values of the scattering angle. These correspond to measurements acquired before and after the backscatter observations.

Aerosol extinction to backscatter ratio from passive satellite measurements

F.-M. Bréon

Title Page	
Abstract	Introduction
Conclusions	References
Tables	Figures
◀	▶
◀	▶
Back	Close
Full Screen / Esc	
Printer-friendly Version	
Interactive Discussion	



Aerosol extinction to backscatter ratio from passive satellite measurements

F.-M. Bréon

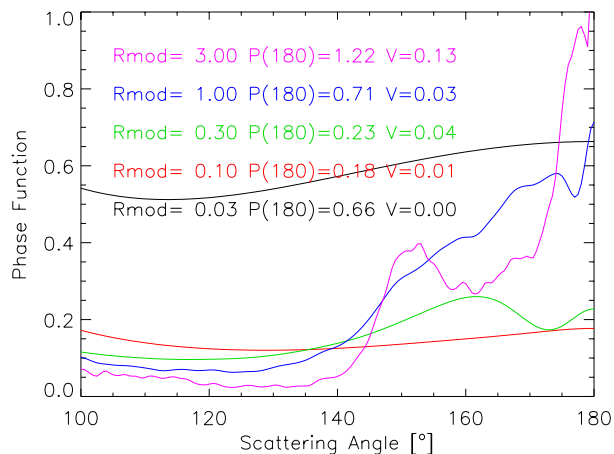


Fig. 3. Results of Mie simulations for a log normal size distribution of width 0.4 and various values of the modal radius (expressed in μm). For these simulations, the wavelength is $0.6 \mu\text{m}$ and the refractive index is 1.4. The slope at backscatter has been computed over the $(173\text{--}180)^\circ$ range as it is similar to POLDER angular sampling.

[Title Page](#)[Abstract](#)[Introduction](#)[Conclusions](#)[References](#)[Tables](#)[Figures](#)[◀](#)[▶](#)[◀](#)[▶](#)[Back](#)[Close](#)[Full Screen / Esc](#)[Printer-friendly Version](#)[Interactive Discussion](#)

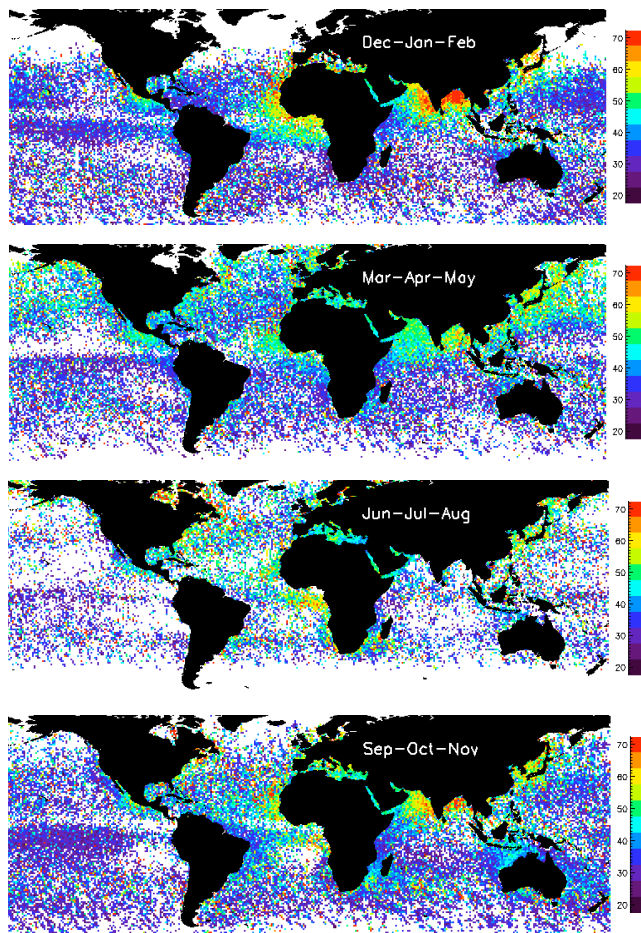


Fig. 4. Seasonal maps of the extinction to backscatter ratio as derived from the Parasol measurements acquired in the backscatter viewing geometry.

Aerosol extinction to backscatter ratio from passive satellite measurements

F.-M. Bréon

Title Page

Abstract Introduction

Conclusions References

Tables Figures

⏪ ⏩

◀ ▶

Back Close

Full Screen / Esc

Printer-friendly Version

Interactive Discussion



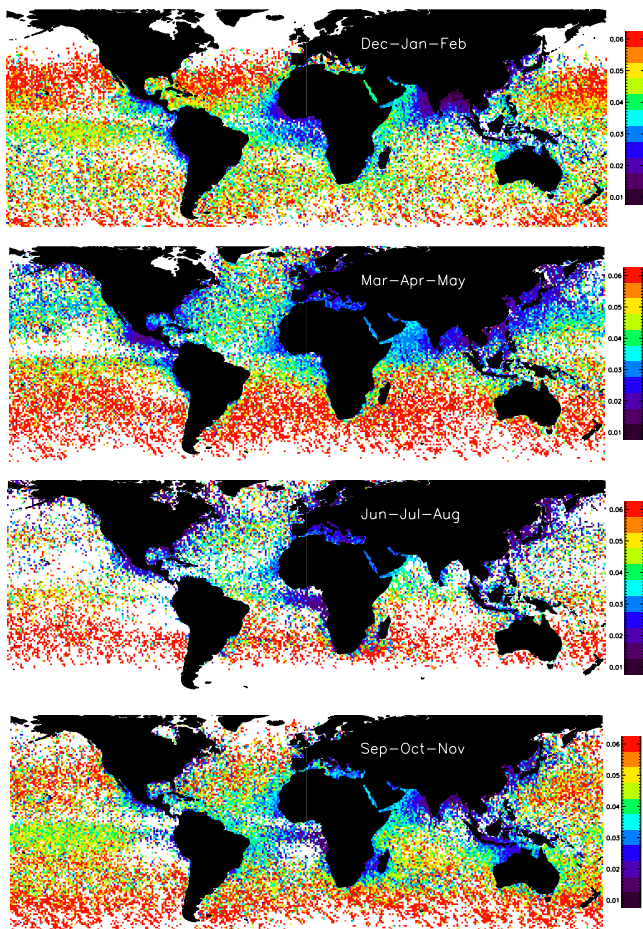


Fig. 5. Same as Fig. 4 but for the phase function slope at backscatter (see Eq. 4).

Aerosol extinction to backscatter ratio from passive satellite measurements

F.-M. Bréon

Title Page

Abstract Introduction

Conclusions References

Tables Figures

⏪ ⏩

◀ ▶

Back Close

Full Screen / Esc

Printer-friendly Version

Interactive Discussion



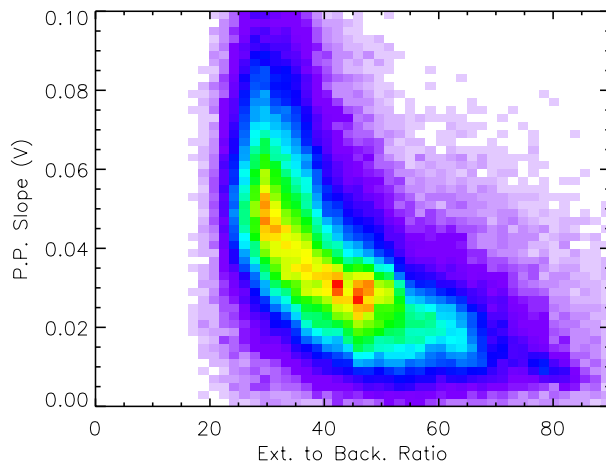


Fig. 6. Bidimensional histogram of the retrieved BER (X-axis) and phase function slope at backscatter as shown in Figs. 4 and 5.

Aerosol extinction to backscatter ratio from passive satellite measurements

F.-M. Bréon

Title Page

Abstract Introduction

Conclusions References

Tables Figures

⏪ ⏩

◀ ▶

Back Close

Full Screen / Esc

Printer-friendly Version

Interactive Discussion

